Wang et al. Nanoscale Research Letters (2016) 11:125
DOI 10.1186/s11671-016-1278-z

Nanoscale Research Letters
a SpringerOpen Journal

NANO EXPRESS Open Access

Surfactant-free Synthesis of CuO with Controllable Morphologies and Enhanced Photocatalytic Property

Xing Wang, Jiao Yang, Liuxue Shi and Meizhen Gao*

Abstract

A green synthesis for nanoleave, nanosheet, spindle-like, rugby-like, dandelion-like and flower-like CuO nanostructures (from 2D to 3D) is successfully achieved through simply hydrothermal synthetic method without the assistance of surfactant. The morphology of CuO nanostructures can be easily tailored by adjusting the amount of ammonia and the source of copper. By designing a time varying experiment, it is verified that the flower- and dandelion-like CuO structures are synthesized by the self-assembly and Ostwald ripening mechanism. Structural and morphological evolutions are investigated by X-ray diffraction (XRD), scanning electron microscopy (SEM) and UV-visible diffuse reflectance spectra. Additionally, the CuO nanostructures with different morphologies could serve as a potential photocatalyst on the photodecomposition of rhodamine B (RhB) aqueous solutions in the presence of H_2O_2 under visible light irradiation.

Keywords: Copper oxide, Ammonia, Morphology, Photocatalytic activity

Background

The photocatalytic performance, electrical and gas-sensing properties are strongly influenced by their morphology and size. Many investigations have been carried out to study the controlling of size, morphology and structure of materials during synthesis [1–4]. To achieve this, the studies of the crystal growth, morphology evolution processes and the corresponding mechanisms are significantly important. As an important p-type transition-metal oxide with a narrow band gap varying between 1.2 and 1.8 eV [5], CuO has been widely studied in thermal conductivity [6], optoelectronic device systems [7], CO oxidation [8], eradication of multi-drug resistant bacteria [9], Li ion batteries anodes [10], heterogeneous catalyst for olefin epoxidation [11], gas sensing [12, 13] and glucose sensor [14–18]. In the past decade, CuO with different morphologies such as nanoribbons [12], microworms [13], nanoplatelets [19], dandelions [20], sandwich [16], nanowires [17], nanotube arrays [21], nanourchins [2, 18] and nanorods [22] have been successfully synthesized through different methods with the assistance of surfactant such as CTAB, PVP, PEG and SDS. Since the surfactants invariably present residual surfactants or organic additives attached to the surfaces of products can block the active sites, it is a serious issue when considering applications in gas sensing or catalysis. Therefore, it is still a challenge to develop new green surfactant-free methods to synthesize well-defined CuO nanostructures [23]. Zhang et al. [24] synthesized flower-like CuO microspheres by a hydrothermal route at 130 °C for 18 h without the assistance of surfactant. Sun et al. [23] synthesized two-dimensional CuO mesoplates and three-dimensinonal CuO mesospindles by an additive-free complex-precursor solution route.

Inspired by the green methods to synthesize various controllable CuO morphologies with surfactant-free building blocks, we present a simply low temperature hydrothermal synthetic method without the assistance of surfactant. And spindle-like, rugby-like, nanoleaves, nanosheets, microspheres and dandelions CuO nanostructures are synthesized through this green method. The synthesis is performed in an ethanol-water mixed solvent using copper source and ammonia as the variable. By designing a time varying experiment, it is verified that the flower- and dandelion-like CuO structures are synthesized

* Correspondence: gaomzlzu@163.com
Key Laboratory for Magnetism and Magnetic Materials of MOE, School of Physical Science and Technology, Lanzhou University, 730000 Lanzhou, People's Republic of China

by the self-assembly and Ostwald ripening mechanism. X-ray diffraction (XRD), scanning electron microscope (SEM) and UV-visible diffuse reflectance spectra are employed to characterize the obtained CuO nanostructures. Furthermore, these copper oxide nanostructures are found to be high qualified photocatalysts for the degradation of rhodamine B (RhB) under visible light irradiation in the presence of hydroxide water (H_2O_2).

Methods

Materials and synthesis

$Cu(NO_3)_2 \cdot 3H_2O$ (Cheng Du Kelong Chemical Reagent Company), $Cu(COOH)_2 \cdot H_2O$ (Tianjin Guangfu Fine Chemical Research Institute), $NH_3 \cdot H_2O$ (25 wt% ~ 28 wt%) (Cheng Du Kelong Chemical Reagent Company) and rhodamin B (RhB) (Tianjin Guangfu Fine Chemical Research Institute) are analytical grade and used without further purification. For a typical CuO nanostructure synthesis, 0.604 g (0.25 mol) of $Cu(NO_3)_2 \cdot 3H_2O$ or 0.5 g (0.25 mol) $Cu(COOH)_2 \cdot H_2O$ mixed solution of 60 mL of deionized water and alcohol (the ratio of alcohol and water is 1:1) and stirred until completely dissolved. At the same time, an appropriate amount of $NH_3 \cdot H_2O$ is added into the above solution quickly and stirred 30 min. The resulting mixture is then transferred into a Teflon-lined steel autoclave and heated in an oven at 80 °C for 10 h. Finally, the precipitates are separated by centrifugation, washed with deionized water and alcohol for several times and dried at 70 °C for 12 h. Through this method, different morphology and size CuO is synthesized by adjusting the amount of $NH_3 \cdot H_2O$ and copper source. The variable parameters are listed in Table 1.

Characterization

Powder XRD pattern is recorded on an X'Pert Philips diffractometer (Cu Kα radiation: λ = 1.5418 Å, 2θ range 20~80°, accelerating voltage 40 kV, applied current 150 mA). The morphology of the products is investigated by field emission scanning electron microscopy (SEM, Hitachi S-4800).

Table 1 The morphologies and synthesis parameters of CuO nanostructures

Sample no.	The amount of $NH_3 \cdot H_2O$ (mL)	Copper source	Morphologies
A	0.5	$Cu(NO_3)_2 \cdot 3H_2O$	Spindle-like
B	0.5	$Cu(COOH)_2 \cdot H_2O$	Rugby-like
C	0.6	$Cu(NO_3)_2 \cdot 3H_2O$	Nanoleave
D	0.6	$Cu(COOH)_2 \cdot H_2O$	Nanosheet
E	1.5	$Cu(NO_3)_2 \cdot 3H_2O$	Dandelion-like
F	1.5	$Cu(COOH)_2 \cdot H_2O$	Flower-like

Photocatalytic properties

The photocatalytic activity of the CuO nanostructures with different morphologies is evaluated by the degradation of a model pollutant RhB under the visible light irradiation with the assistance of hydrogen peroxide (H_2O_2) at ambient temperature. The original solution is prepared by mixing 5 mL H_2O_2 (30 wt%), 50 mL RhB solution (10^{-5} M) and 20 mg copper oxide powder together and then stirred in the dark for 60 min to ensure an adsorption-desorption equilibrium is established. Afterwards, the dispersion is irradiated by a 350-W xenon lamp equipped with a filter cutoff (λ ≥420 nm) under magnetic stirring. At given time intervals, the dispersion is sampled and centrifuged to separate the catalyst. The adsorption spectrum of the solution is then recorded with an UV-visible spectrophotometer (Shimadzu UV-3600).

Results and discussion

Crystal structures of the prepared CuO nanomaterials

Figure 1 shows the XRD patterns of the products under different reaction conditions after hydrothermal treatment. Diffraction peaks are observed at 2θ of 32.5°, 35.5°, 38.7°, 48.7°, 53.7°, 58.2°, 61.5°, 66.3°, 68°, 72.3° and 74.8°. These peaks can be assigned to the (110), (002), (111), (-202), (020), (-113), (-311), (220), (311) and (-222) planes of monoclinic CuO (JCPDS 65-2309). No peaks of impurities such as copper hydroxide or other copper compounds can be detected, suggesting the high purity and similarity of all the as-prepared products.

Morphologies of CuO nanostructures synthesized by $Cu(NO_3)_2$ as a copper source

When 0.5 mL of $NH_3 \cdot H_2O$ is added in the reaction system, CuO nanostructure with a spindle-like morphology is produced as shown in Fig. 2a and Fig. 2b. We can see that the CuO nanostructures are about 600 nm in length

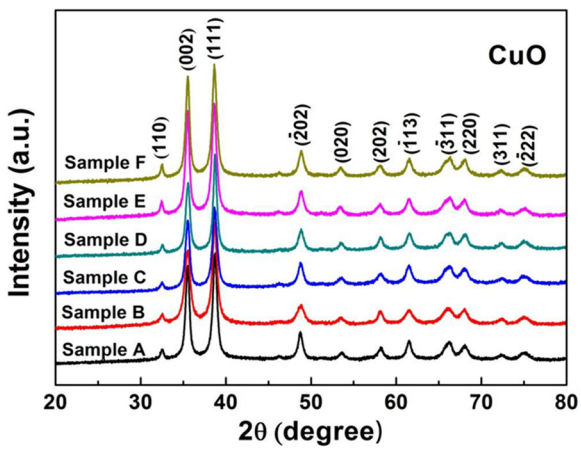

Fig. 1 XRD patterns of CuO nanostructures after hydrothermal treatment with different reaction conditions

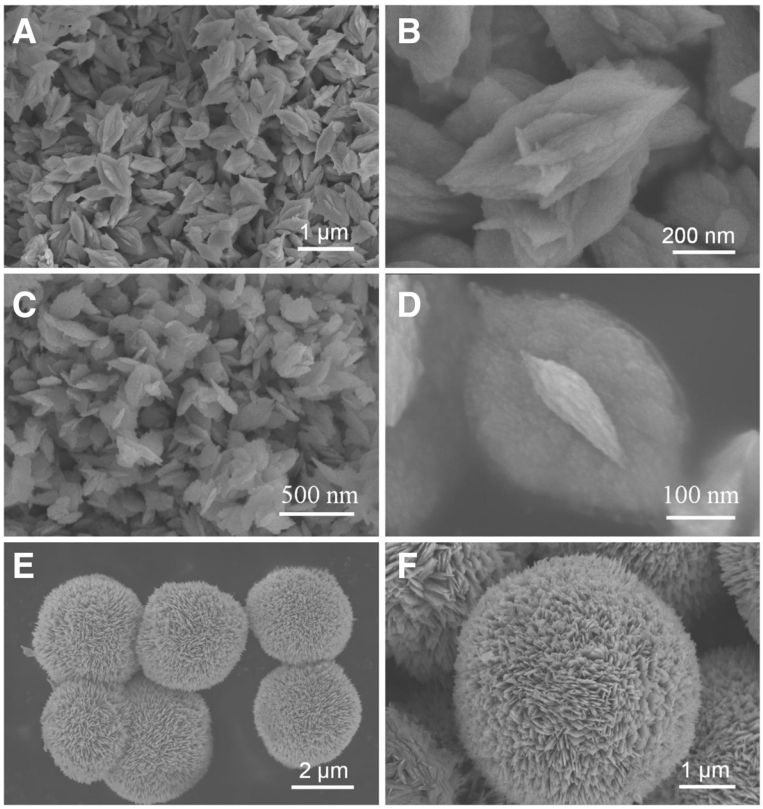

Fig. 2 Electron microscopy images of CuO obtained by different amount of ammonia: **a**, **b** sample A; **c**, **d** sample C; **e**, **f** sample E

and 300 nm in width. When the volume of the $NH_3 \cdot H_2O$ is increased to 0.6 mL, the centre of the spindle-like CuO is getting thinner and finally obtains a large number of nanoleaves (Fig. 2c, d). The CuO nanostructures are about 250 nm in length and 130 nm in width. Further increase $NH_3 \cdot H_2O$ to 1.5 mL, 3D dandelion-like CuO with hierarchical nanostructures is obtained (Fig. 2e, f). The diameter of the CuO is about 4 μm. As can be seen from the SEM, the dandelion-like CuO is consisted of nanosheets (Fig. 2f). But further increases in the amount of $NH_3 \cdot H_2O$, the morphology and size of the CuO do not change significantly, all the products remain dandelion-like.

Morphologies of CuO nanostructures synthesized by $Cu(COOH)_2$ as a copper source

When 0.5 mL of $NH_3 \cdot H_2O$ is added in the reaction system, CuO nanostructures with rugby-like morphology are produced as shown in Fig. 3a and Fig. 3b. The CuO nanostructures are about 200 nm in length and 130 nm in width. When the volume of the $NH_3 \cdot H_2O$ is increased to 0.6 mL, a large number of nanosheets with about 150 nm in length and 100 nm in width can be obtained (Fig. 3c, d). When the amount of the $NH_3 \cdot H_2O$ is increased to 1.5 mL, 3D flower-like CuO microstructures consisted of nanosheets with the diameter about 3 μm can be obtained (Fig. 3e, f). The accumulation of nanosheets of dandelion-like CuO is denser than the flower-like CuO, and the diameter of dandelion-like CuO is larger than that of flower-like CuO. Further increase the amount of $NH_3 \cdot H_2O$, the morphology and size of the CuO do not change anymore, all the products remain flower-like CuO microstructures.

Plausible mechanisms for the formation of CuO nanostructures

When 0.5 mL or 0.6 mL ammonia is added in to the solution, a flocculent precipitation is generated in these blue solutions. The precursor in the blue solution before heat treatment is $Cu(OH)_2$. Copper oxide is obtained after heat treats the $Cu(OH)_2$ precipitation; the reactions can be summarized as follows:

$$Cu^{2+} + 2NH_3 \cdot H_2O \rightarrow Cu(OH)_2\downarrow + 2NH_4^+ \quad (1)$$

$$Cu(OH)_2 \xrightarrow{80^\circ C} CuO + H_2O \quad (2)$$

Increase the dose of ammonia further, the firstly formed flocculent precipitate dissolved. Then $[Cu(NH_3)_4]^{2+}$ can

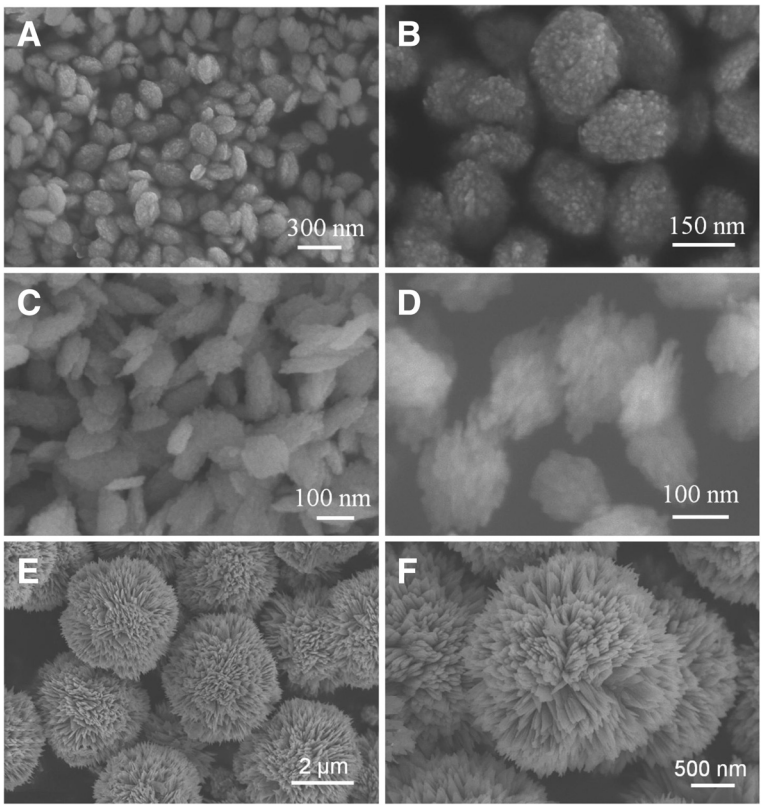

Fig. 3 SEM images of CuO obtained by different volume of ammonia: **a**, **b** sample B; **c**, **d** sample D; **e**, **f** sample F

be considered as the precursor entity for the formation of CuO. The reactions can be described as follows:

$$Cu^{2+} + 4NH_3 \cdot H_2O \rightarrow \left[Cu(NH_3)_4\right]^{2+} + 2OH^- + 4H_2O \quad (3)$$

$$\left[Cu(NH_3)_4\right]^{2+} + 2OH^- \overset{80^\circ C}{\rightarrow} CuO + 4NH_3 + H_2O \quad (4)$$

In the present case, CuO particles are synthesized directly by the decomposition of $Cu(OH)_2$ or $(Cu(NH_3)_4)^{2+}$ precursor under hydrothermal conditions without the presence of various surfactant. The crystal formation process can be divided into two stages: nucleation and crystal growth. When the amount of ammonia is less than 0.6 mL, $Cu(OH)_2$ is formed in aqueous reaction medium, which transformed into CuO under hydrothermal conditions [Eqs. (1) and (2)]. When the amount of ammonia is over 1.5 mL, the soluble $[Cu(NH_3)_4]^{2+}$ complex is formed, which transformed into CuO under hydrothermal conditions [Eqs. (3) and (4)]. The different growth unite might affect the competition between thermodynamics and kinetics during the reduction of precursors and nucleation and growth of CuO crystals [25]. Comparing Fig. 2 with Fig. 3, we can conclude that the morphologies of CuO are not the same and the sizes of CuO become smaller when the copper source changes from $Cu(NO_3)_2$ to $Cu(COOH)_2$. The effect of copper source on the structure of CuO may be that the NO_3^- is inorganic strong acid root and the $COOH^-$ is organic weak acid root; in the synthesis of complex precipitation, the anions in the solution affect the nucleation and growth of the copper oxide precursor. From the above analysis, it is safe to say that the ammonia and the acid radical ion have an important effect on the formation of CuO morphology.

Both self-assembly and Ostwald ripening mechanism are involved in the process of synthesizing of the dandelion-like and flower-like CuO. To verify this, the time-dependant morphologies of the dandelion- and flower-like CuO are shown in Fig. 4. We can conclude that after 3 h, CuO microspheres are formed by the self-assembly of particles, but the surface of microspheres is uneven; there are still many small particles attached to the surface of microspheres (Fig. 4a, d). With the extension of reaction time, these particles gradually ripe and the final structures are formed (Fig. 4c, f).

Photochemical performances

The optical energy band gaps of semiconductors are found to be dependent on their microstructures, so the

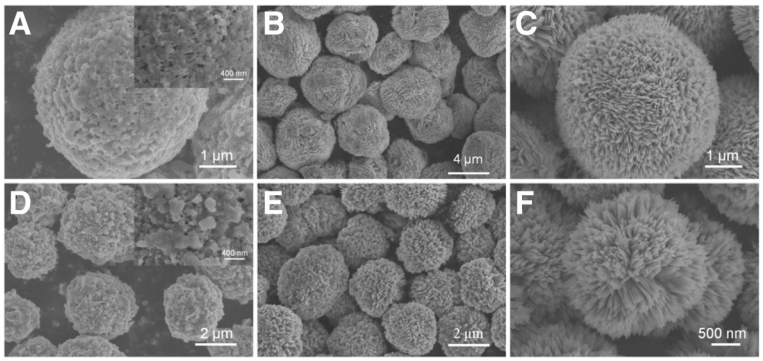

Fig. 4 SEM images of CuO obtained after different reaction time: **a**, **d** 3 h; **b**, **e** 5 h; **c**, **f** 10 h

above as-prepared CuO nanostructures with different morphologies are investigated by UV-vis spectra. Figure 5a shows the UV-visible spectra of as-prepared CuO products with different morphologies, the absorption edges of spindle-like, rugby-like, nanoleave, nanosheet, dandelion-like and flower-like CuO occur at 975, 1010, 985, 910, 1000 and 960 nm, respectively. Figure 5b shows the plot of photon energy; we can find that the band gaps of spindle-like, rugby-like, nanoleave, nanosheet, dandelion-like and flower-like CuO are estimated to be 1.27, 1.23, 1.26, 1.36, 1.24 and 1.29 eV, respectively. The effect of the morphology of CuO nanostructure is clearly noted on its band gap. The fundamental photodegradation mechanism involves the acceleration in decomposition of H_2O_2 over CuO crystals to generate free radical species, such as .OH, .OOH or $.O_2^-$, which are deemed to be liable for the degradation of the dyes. The related chemical reactions include the electrons (e^-) in the VB can be excited to the CB and at the same time generate the same number of holes (h^+) in the VB. The formed e^- and h^+ pairs can be captured by H_2O_2 molecules leading to the formation of .OH, .HOO or $.O_2^-$ [Eqs. (5)–(8)]; oxidant species react with dye then finally realize complete mineralization with the formation of CO_2, H_2O or other inorganic ion [23].

$$CuO + h\nu \rightarrow h_{vb+} + e_{cb^-} \quad (5)$$

$$H_2O_2 + h_{vb+} \rightarrow \cdot OOH + H^+ \quad (6)$$

$$H_2O_2 + e_{cb^-} \rightarrow \cdot OH + OH^- \quad (7)$$

$$\cdot OOH \rightarrow \cdot O_2^- + H^+ \quad (8)$$

To explore the photochemical performances of the as-prepared CuO nanostructures, photocatalytic activity of CuO is evaluated in the oxidation of RhB under visible light irradiation at ambient temperature in the presence of hydroxide water (H_2O_2). The characteristic absorption pick at 554 nm of RhB is monitored to follow the catalytic degradation process. Figure 6a shows the optical absorption spectra of RhB measured at different intervals in the absence of catalysts and H_2O_2; only a slight degradation (2.2 %) of RhB can be detected after 100 min (Fig. 6i, *A*). Figure 6b shows the optical absorption spectra of RhB measured at different intervals only with the H_2O_2; only 7.4 % of RhB can be detected after

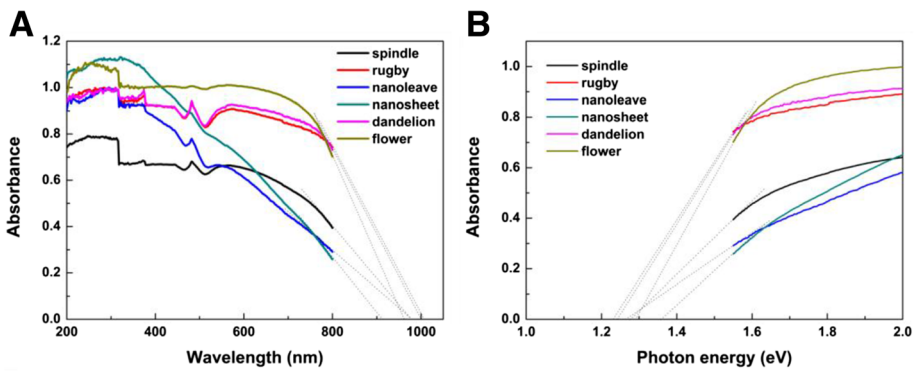

Fig. 5 a UV-vis spectra and (**b**) plot of photon energy of as-prepared CuO products with different morphologies

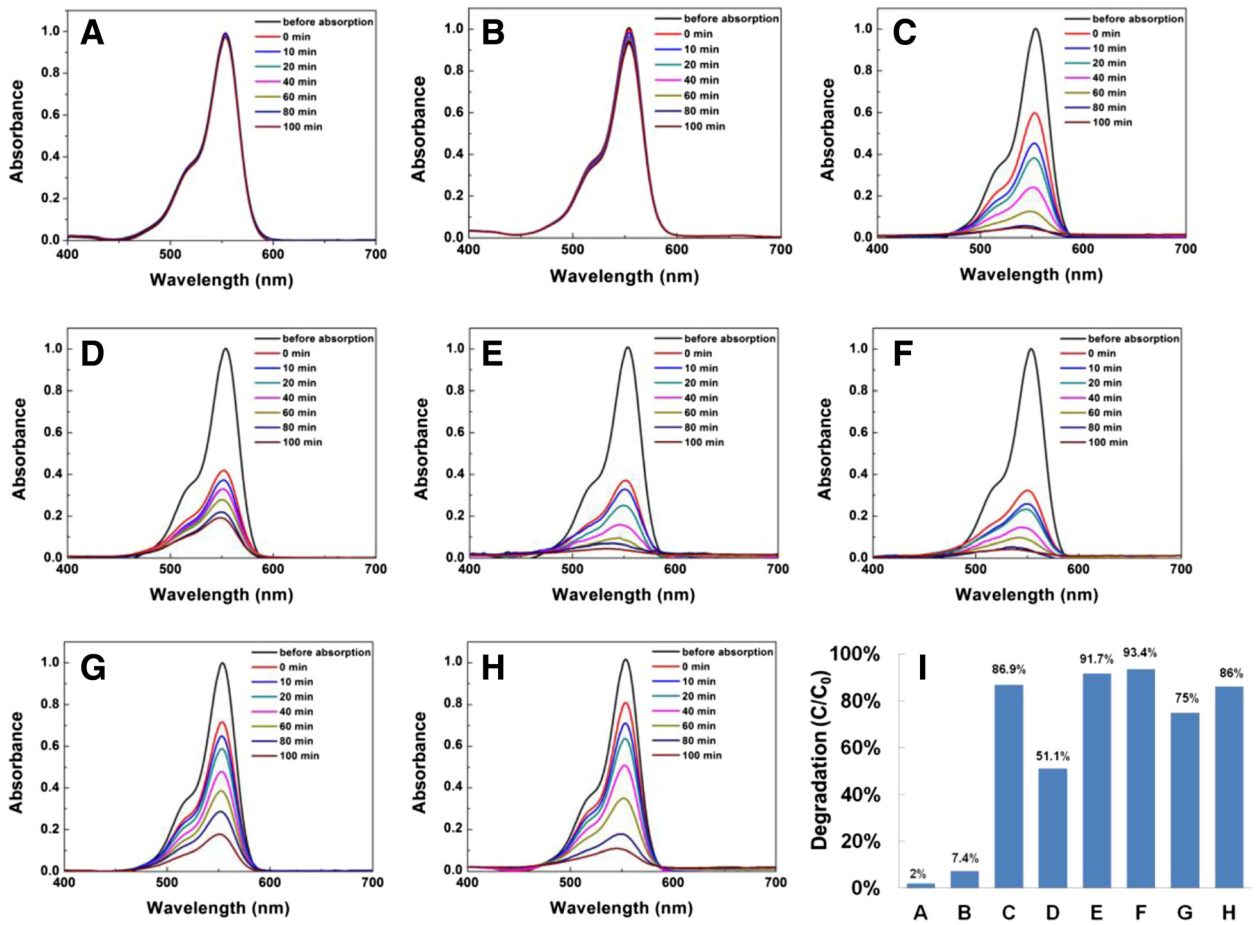

Fig. 6 Absorption spectra of RhB under visible light irradiation with different CuO nanostructures. **a** Without any catalyst and H_2O_2, **b** only with H_2O_2, **c** with sample A, **d** with sample B, **e** with sample C, **f** with sample D, **g** with sample E, **h** with sample F, and **i** plot of the extent of photodegradation of RhB which corresponds to *A*, *B*, *C*, *D*, *E*, *F*, *G* and *H*

100 min (Fig. 6i, *B*). Figure 6c–h shows the optical absorption spectra of RhB tested at different intervals in the presence of different nanostructured CuO. It can be found that the degradation rate of nanoleave and nanosheet CuO are both very fast, 91.7 and 93.4 % are reached respectively after 100 min (Fig.6i, *E*, *F*). The lowest degradation rate is about 51.1 % by the rugby-like CuO (Fig. 6i, *D*). The degradation of RhB at 100 min in the presence of above six samples is as follows: nanosheet CuO (93.4 %) > nanoleave CuO (91.7 %) > spindle-like CuO (86.9 %) > flower-like CuO (86 %) > dandelion-like (75 %) > rugby-like (51.1 %).

Conclusions

In summary, a green synthesis for spindle-like, rugby-like, nanoleave, nanosheet, dandelion-like and flower-like CuO nanostructures (from 2D to 3D) are successfully achieved through simply hydrothermal synthetic method without the assistance of surfactant. The formation of CuO nanostructures here is basically effected by the amount of ammonia and the copper source. We also found that the flower- and dandelion-like CuO structures are synthesized by the self-assembly and the Ostwald ripening mechanism. Additionally, the CuO nanostructures with different morphologies could serve as a potential photocatalyst on the photodecomposition of RhB aqueous solutions in the presence of H_2O_2 under visible light irradiation.

Competing interests

The authors declare that they have no competing interests.

Authors' contributions

XW conceived the study, carried out the acquisition, analyzed and interpreted the data, performed the sequence alignment, and drafted the manuscript. JY and LS helped to revise the manuscript. MG helped to revise the manuscript critically for important intellectual content. All authors have read and approved the final manuscript.

Acknowledgements

This work was financially supported by the NSFC (No. 51371093) and the MOE (No. IRT1251 & 20130211130003) of China.

Received: 5 December 2015 Accepted: 25 January 2016
Published online: 03 March 2016

References

1. Anders CB, Chess JJ, Wingett DG, Punnoose A (2015) Serum proteins enhance dispersion stability and influence the cytotoxicity and dosimetry of ZnO nanoparticles in suspension and adherent cancer cell models. Nanoscale Res Lett 10:448
2. Xu LP, Sithambaram S, Zhang YS, Chen CH, Jin L, Joesten R, Suib SL (2009) Novel urchin-like CuO synthesized by a facial reflux method with efficient olefin epoxidation catalytic performance. Chem Mater 21: 1253–1259
3. Li L, Dai HT, Feng LF, Luo D, Wang SG, Sun XW (2015) Enhance photoelectrochemical hydrogen-generation activity and stability of TiO_2 nanorod arrays sensitized by PbS and CdS quantum dots under UV-visible light. Nanoscale Res Lett 10:418
4. Chen HM, He JH, Zhang CB, He H (2007) Self-assembly of novel mesoporous manganese oxide nanostructure and their application in oxidative decomposition of formaldehyde. J Phys Chem C 111: 18033–18038
5. Hansen BJ, Koukin N, Lu GH, Lin IK, Chen JH, Zhang X (2010) Transport, analyte detection, and opto-electronic response of p-type CuO nanowires. J Phys Chem C 114:2440–2447
6. Yu W, Zhao JC, Wang MZ, Hu YH, Chen LF, Xie HQ (2015) Thermal conductivity enhancement in thermal grease containing different CuO structures. Nanoscale Res Lett 10:113
7. Luo LB, Wang XH, Xie C, Li ZJ, Lu R, Yang XB, Lu J (2014) One-dimensional CuO nanowire: synthesis, electrical, and optoelectronic devices application. Nanoscale Res Lett 9:637
8. Feng YZ, Zheng XL (2010) Plasma-enhanced catalytic CuO nanowires for CO oxidation. Nano Lett 10:4762–4766
9. Malka E, Perelshtein L, Lipovsky A, Shalom Y, Naparshek L, Perkas N et al (2013) Eradication of multi-drug resistant bacteria by a novel Zn-doped CuO nanocomposite. Small 9:4069–4076
10. Ko S, Lee JI, Yang HS, Park S, Jeong U (2012) Mesoporous CuO particles threaded with CNTs for high-performance lithium-ion battery anodes. Adv Mater 24:4451–4456
11. Zhu MY, Diao GW (2012) High catalytic activity of CuO nanorods for oxidation of cyclohexene to 2-cyclohexene-1-one. Catal Sci Technol 2:82–84
12. Gou XQ, Wang GX, Yang J, Park J, Wexler D (2008) Chemical synthesis, characterisation and gas sensing performance of copper oxide nanoribbons. J Mater Chem 18:965–969
13. Liu XH, Zhang J, Kang YF, Wu SH, Wang SR (2012) Brochantite tabular microspindles and their conversion to wormlike CuO structures for gas sensing. CrystEngComm 14:620–625
14. Li CL, Yamahara H, Lee Y, Tabata H, Delaunay JJ (2015) CuO nanowire/microflower/nanowire modified Cu electrode with enhanced electrochemical performance for non-enzymatic glucose sensing. Nanotechnology 26:305503
15. Li CL, Yamahara H, Lee Y, Tabata H, Delaunay JJ (2015) Nanoporous CuO layer modified Cu electrode for high performance enzymatic and non-enzymatic glucose sensing. Nanotechnology 26:015503
16. Meher SK, Rao GR (2013) Archetypal sandwich-structured CuO for high performance non-enzymatic sensing of glucose. Nanoscale 5:2089–2099
17. Huang JF, Zhu YH, Yang XL, Chen W, Zhou Y, Li CZ (2015) Flexible 3D porous CuO nanowire arrays for enzymeless glucose sensing: in situ engineered versus ex situ piled. Nanoscale 7:559–569
18. Sun SD, Zhang XZ, Sun YX, Zhang J, Yang SC, Song XP, Yang ZM (2013) A facile strategy for the synthesis of hierarchical CuO nanourchins and their application as non-enzymatic glucose sensors. RSC Adv 3:13712–13719
19. Zou GF, Li H, Zhang DW, Xiong K, Dong C, Qian YT (2006) Well-aligned arrays of CuO nanoplatelets. J Phys Chem B 110:1632–1637
20. Liu B, Zeng HC (2004) Mesoscale organization of CuO nanoribbons: formation of "dandelions". J Am Chem Soc 126:8124–8125
21. Chun SR, Sasangka WA, Ng MZ, Liu Q, Du A, Zhu J, Ng CM, Liu ZQ, Chiam SY, Gan CL (2013) Joining copper oxide nanotube arrays driven by the nanoscale Kirkendall effect. Small 9:2546–2552
22. Chen LJ, Li LP, Li GS (2008) Synthesis of CuO nanorods and their catalytic activity in the thermal decomposition of ammonium perchlorate. J Alloys Compd 464:532–536
23. Sun SD, Zhang XZ, Zhang J, Wang LQ, Song XP, Yang ZM (2013) Surfactant-free CuO mesocrystals with controllable dimensions: green ordered-aggregation-driven synthesis, formation mechanism and their photochemical performances. CrystEngComm 15:867–877
24. Zhang ZL, Che HW, Wang YL, Gao JJ, She XL, Sun J, Zhong ZY, Su FB (2012) Flower-like CuO microspheres with enhanced catalytic performance for dimethyldichlorosilane synthesis. RSC Adv 2:2254–2256
25. Pacholski C, Kornowski A, Welle H (2002) Self-assembly of ZnO from nanodots to nanorods. Angew Chem Int Ed 41:1188–1191